Spin-split electronic states in graphene: Effects due to lattice deformation, Rashba effect, and adatoms by first principles

Samir Abdelouahed, A. Ernst, and J. Henk
Max-Planck-Institut für Mikrostrukturphysik, Weinberg 2, Halle, D-06120 Saale, Germany

I. V. Maznichenko
Institut für Physik, Martin-Luther-Universität Halle-Wittenberg, Halle, D-06099 Saale, Germany

I. Mertig
Max-Planck-Institut für Mikrostrukturphysik, Weinberg 2, Halle, D-06120 Saale, Germany
and Institut für Physik, Martin-Luther-Universität Halle-Wittenberg, Halle, D-06099 Saale, Germany
(Received 18 May 2010; revised manuscript received 13 August 2010; published 14 September 2010)

The spin-dependent electronic structure of graphene is investigated by first-principles calculations, using relativistic full-potential linearized augmented plane wave and Korringa-Kohn-Rostoker methods. Our systematic study addresses various effects on the electronic states at the Dirac points: in-plane and out-of-plane deformation of graphene's honeycomb lattice, external electric fields, doping and band filling due to heavy and magnetic adatoms (Au and Ni). Having revealed the underlying mechanisms, our findings open a route to manufacture graphene with sizable spin splittings.

DOI: 10.1103/PhysRevB.82.125424 PACS number(s): 73.22.Pr, 73.20.−r, 71.70.Ej, 75.70.−i

I. INTRODUCTION

Graphene is a unique material due to the linear dispersing bands at the Fermi level.[1] Being a monatomic sheet of carbon arranged in a honeycomb structure, it is the building block of many carbon-based materials; just to name a few, graphite, carbon nanotubes, and C_{60} molecules. Its two-dimensional carriers mobility is very high[2] and, therefore, graphene is considered as a promising element in next-generation electronic devices, e.g., the quantum Hall effect[3] and the spin Hall effect.[4] Consequently, it is investigated both in experiment and in theory with great effort.

Another hot topic in contemporary physics is spin electronics or spintronics for short. Here, one major aim is to control the spins of the conducting electrons by an external electric field via either magnetoelectric coupling or by the spin-orbit (SO) interaction. The latter approach is intimately associated with the Rashba-Bychkov effect[5] which shows up in semiconductor heterostructures and at metal surfaces.[6–9] Since it is due to breaking the spatial inversion symmetry, it gives rise to an extrinsic SO splitting.

In view of the former, it is obvious to combine the established Rashba-type spin-orbit splitting with graphene's extraordinary electronic properties.[10] However, the Rashba effect at surfaces relies on heavy elements, such as Au and Bi, to achieve a sizable spin splitting. Carbon, in contrast, is a light element and its intrinsic SO coupling is thus tiny. Therefore, there is an ongoing quest to increase the SO splitting in graphene by other means. The main mechanism to come into play are, first, lattice deformations which open new "interaction channels" between the otherwise uncoupled σ and π orbitals of graphene. Second, external electric fields allow to induce a Rashba-type spin splitting, while, third, adatoms could increase the important d-orbital contribution to the spin-orbit coupling and alter the band filling in the graphene layer. Fourth, magnetic adatoms could induce an exchange-mediated spin splitting.

We report on a systematic and comprehensive first-principles investigation of all of the four mechanisms mentioned above. By performing independent relativistic full-potential linearized augmented plane wave (FLAPW) and Korringa-Kohn-Rostoker calculations (KKR), reliable conclusions on the spin-orbit and exchange-induced effects in graphene can be drawn.

The paper is organized as follows. In Sec. II we provide details of the computational methods. Section III is devoted to the effect of in-plane lattice deformations. In Sec. IV, the Rashba effect in perfect and buckled graphene is discussed. In Sec. V, we deal with the doping graphene by Au and Ni adatoms. The results are put into a broader context in Sec. VI.

II. COMPUTATIONAL DETAILS

The first-principles calculations in the present work were performed using FLAPW and KKR methods. For both, the lattice constant was chosen as $\sqrt{3}a=4.64a_0$ (Bohr radii).

The FLAPW calculations rely on the FLEUR code[11] with Moruzzi-Janak-Williams parametrization of the exchange-correlation potential.[12] The muffin-tin radii R_{mt} are set to $1.3a_0$ for C, $2.0a_0$ for Ni, and $2.2a_0$ for Au, respectively. The cutoff for the plane-wave basis is set to $K_{\max}=4.0a_0^{-1}$ while both the charge density and potential cutoffs are $G_{\max}=13.0a_0^{-1}$. The wave functions, charge density, and the potential inside the muffin-tin spheres were expanded in angular momentum up to $l_{\max}=6$ for C and $l_{\max}=8$ for both Ni and Au. The spin-orbit coupling is treated self-consistently in a second-variational scheme.[13] Whenever not explicitly stated, the spin-quantization axis is chosen parallel to the graphene surface and perpendicular to the wave vector $\vec{k}_{\parallel}$.

Within FLEUR, an external electric field is simulated by a capacitor, that is, two sheets of opposite charge placed on both sides of the graphene layer; here: at a distance of $10a_0$ (Fig. 1).

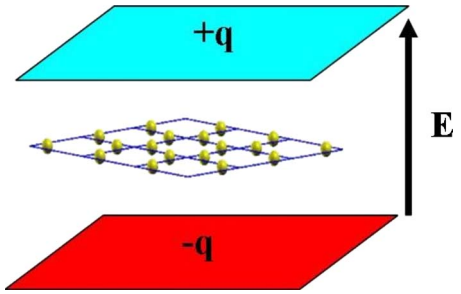

FIG. 1. (Color online) Schematic of the electric field implementation in FLAPW. The graphene layer (center) is sandwiched by a capacitor with charges $\pm q$ which imposes a transverse electrostatic field.

The external electric field imposes an additional (extrinsic) contribution to the SO coupling, that is, the Rashba effect. In FLAPW, both the intrinsic (atomic) and the extrinsic (Rashba) contributions are fully captured. To be more precise, both charge density and Coulomb potential are calculated self-consistently without shape approximation; in particular, both account for the external electric field. The spin-orbit interaction is considered only within the muffin-tin spheres whose potentials are affected by the external electric field. As a consequence, the extrinsic SO interaction is indirectly included.

The FLAPW calculations are accompanied by completely independent first-principles KKR and relativistic layer-KKR calculations,[14,15] utilizing the Perdew-Wang exchange-correlation functional.[16] Because graphene's geometry is rather open, an additional empty muffin-tin sphere has been placed within the two-dimensional unit cell. Likewise, the two semi-infinite vacuum regions are described by empty spheres. The sphere radii are $1.4809a_0$, $l_{\max}=4$.

Although the KKR calculations do not employ the full (nonspherical) potential, their results compare favorable with those of the FLAPW calculations. For example, the strengths of the intrinsic spin-orbit coupling of graphene differ by less than 0.5 μeV. Thus, we report in this paper exclusively on the FLAPW calculations, with the exception of the spin structure shown in Fig. 5.

III. STRUCTURAL TRANSITION FROM THE HONEYCOMB TOWARD A SQUARE LATTICE

Graphene can be manufactured by exfoliation[17] or by thermal graphitization of SiC.[18] It is usually strained[19] when grown on a substrate, with its detailed geometry depending on the terminating layer of the substrate. In any case, a deviation from the perfect honeycomb lattice alters the electronic properties of graphene. In order to gain insight into electronic properties of deformed graphene, we consider a transition from the honeycomb lattice toward a square lattice, in analogy to the fcc-to-bcc transition along Bain's path.[20]

The transformation from the honeycomb to the square lattice is described by lattice vectors

$$\vec{a}_1 = \frac{1}{2}\begin{pmatrix} U(\sqrt{3}-\sqrt{\sqrt{3}})+\sqrt{\sqrt{3}} \\ -U(1-\sqrt{\sqrt{3}})-\sqrt{\sqrt{3}} \end{pmatrix},$$

$$\vec{a}_2 = \frac{1}{2}\begin{pmatrix} U(\sqrt{3}-\sqrt{\sqrt{3}})+\sqrt{\sqrt{3}} \\ U(1-\sqrt{\sqrt{3}})+\sqrt{\sqrt{3}} \end{pmatrix} \quad (1)$$

and basis vectors

$$\vec{\tau}_A = \begin{pmatrix} (1-U)\dfrac{\sqrt{\sqrt{3}}}{4}+\dfrac{\sqrt{3}}{6}U \\ 0 \end{pmatrix}, \vec{\tau}_B = -\begin{pmatrix} (1-U)\dfrac{\sqrt{\sqrt{3}}}{4}+\dfrac{\sqrt{3}}{6}U \\ 0 \end{pmatrix}. \quad (2)$$

$U=1$ ($U=0$) corresponds to the honeycomb (square) lattice, A and B denote the sublattices [Fig. 2(a)]. While the area of the unit cell is constant, the number of nearest neighbors increases from three for the honeycomb lattice to four in the square lattice.

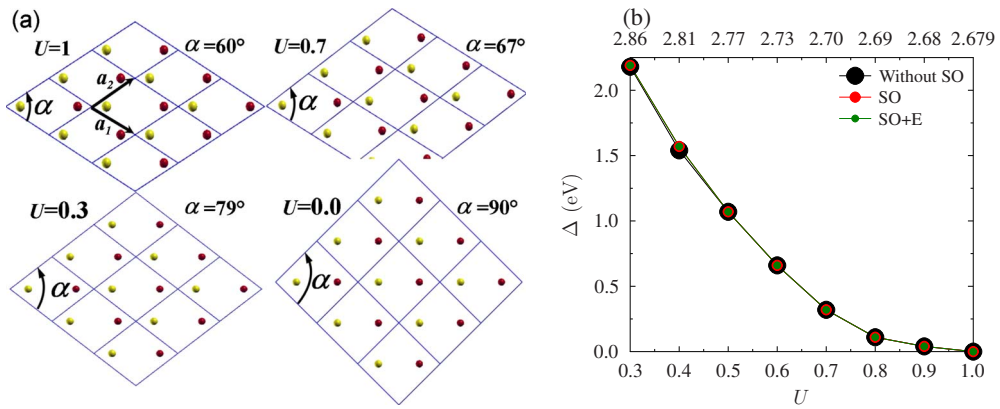

FIG. 2. (Color online) (a) Transition from the honeycomb to the square lattice. The graphene layer is snapshot for $U=1.0$, 0.7, 0.3, and 0.0 [cf. Eqs. (1) and (2)]. Yellow (light gray) and red (dark gray) spheres distinguish the A and B sublattices. The angle α between the basis vectors $\vec{a}_1$ and $\vec{a}_2$ is given in addition. (b) Width Δ of the fundamental band gap at K (K') of the two-dimensional Brillouin zone versus U. Δ is shown for calculations without spin-orbit coupling ("Without SO," large, black), with spin-orbit coupling ("SO," medium-sized, red), as well as with spin-orbit coupling and an external electric field of 0.1 V/Å ("SO+E," small, green), respectively. The top abscissa indicates the nearest-neighbor distance (in Bohr radii).

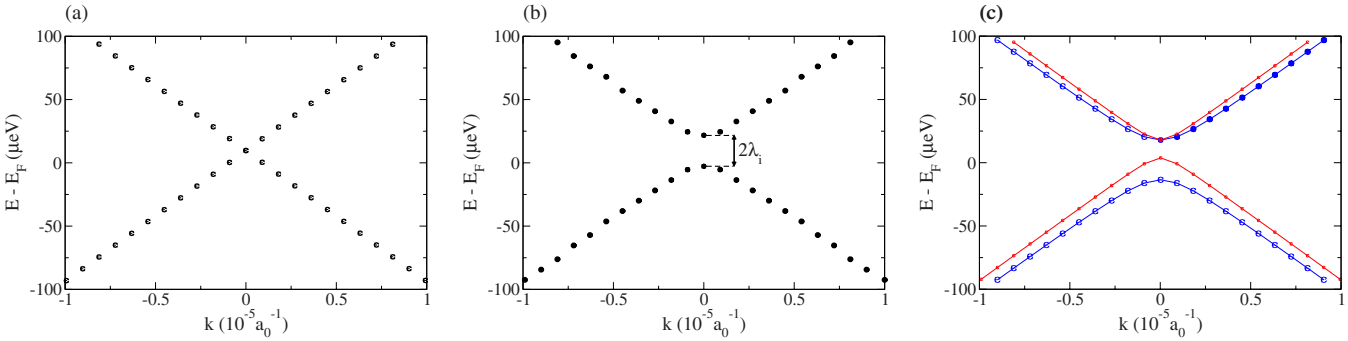

FIG. 3. (Color online) Band structure of graphene near the Dirac point K (K') (a) without SO coupling and without external electric field, (b) including SO coupling and without electric field, and (c) including SO coupling and an external electric field of 0.1 V/Å. In (c), lines depict the model band structure, Eq. (5), whereas red small and blue big symbols represent the $\mu=1$ and $\mu=-1$ branches obtained from the self-consistent calculations, respectively.

The width Δ of the fundamental gap increases with deformation from the honeycomb [$U=1$ in Fig. 2(b)] toward the square lattice ($U\rightarrow 0$). This is explained by the increasing binding energy of the σ orbitals with a transformation of graphene's sp^2 hybridization to a p^2 hybridization.

With regard to this finding, a fundamental gap at K (K') could hint toward a structural deformation of the graphene lattice. An experimental Δ of 0.26 eV, as reported for graphene on SiC,[21] would correspond to $U\approx 0.73$ [Fig. 2(b)], with a nearest-neighbor distance of $2.696a_0$.

The band gap is neither significantly affected by spin-orbit coupling nor by a moderate external electric field, which is evident by comparing the respective data in Fig. 2(b). As we shall discuss in the following, effects of the SO interaction are within the order of microelectron volt, rather than in electron volt.

IV. RASHBA EFFECT IN GRAPHENE

One of the major challenges in spintronics is to find means to manipulate efficiently the electrons' spins by an external electric field. For example, in a spin field-effect transistor,[22] the Rashba effect in a two-dimensional electron gas which is confined at a semiconductor heterostructure is controlled by a gate voltage. In view of its exceptional transport properties, it is obvious to study the Rashba effect in graphene as well. In *ab initio* calculations, the latter could be imposed by an external electric field, as is described in Sec. II and sketched in Fig. 1.

With respect to device applications, a sizable Rashba splitting is desirable. Experimental and theoretical investigations of the Rashba effect in surface states at metal surfaces have shown that an inevitable prerequisite for this splitting is a large atomic spin-orbit coupling.[23] This is why the L-gap surface states in Au(111) ($Z_{\mathrm{Au}}=79$) show a clear spin splitting while their counterparts in Cu(111) ($Z_{\mathrm{Cu}}=27$) do not. Given the small atomic number of carbon ($Z_{\mathrm{C}}=6$), one can thus expect a tiny spin splitting, unless an additional effect would increase the latter considerably. Among the mechanisms which could increase the Rashba-type splitting in graphene substrate-mediated effects are of particular importance: bending, buckling of the carbon layer, as well as electron and hole doping.

According to the effective-mass model,[24] the SO interaction in graphene can be split into an intrinsic and an extrinsic contribution.[25] The intrinsic reads

$$H_{\mathrm{SO}}^{\mathrm{int}}=\lambda_{\mathrm{i}}\psi^{+}\sigma_z\tau_z s_z\psi, \tag{3}$$

where the Pauli matrix σ_z describes electronic states on the sublattice A or B. The Pauli matrix τ_z describes states at K or K'. λ_{i} quantifies the strength of the intrinsic SO coupling. The extrinsic contribution reads

$$H_{\mathrm{SO}}^{\mathrm{ext}}=\lambda_{\mathrm{R}}\psi^{+}(\sigma_x\tau_z s_y-\sigma_y s_x)\psi, \tag{4}$$

where λ_{R} is the strength of the Rashba SO coupling.[5] The Rashba terms (in parenthesis) are due to the breaking of the inversion symmetry which is mediated by the external electric field. The eigenvalues of the joint Hamiltonian are

$$\varepsilon_{\mu\nu}=\mu\lambda_{\mathrm{R}}+\nu\sqrt{(\hbar v_{\mathrm{F}}k)^2+(\lambda_{\mathrm{R}}-\mu\lambda_{\mathrm{i}})^2}, \tag{5}$$

where $\mu,\nu=\pm 1$ index the conduction and valence bands near the K (K') Dirac points. k is taken with respect to K or K' and v_{F} is the Fermi velocity of the linear bands (without SO coupling).

In this section we report on the band topology in graphene which is subject to an external electric field. First, we study the electric field effect on an ideal graphene monolayer (Sec. IV A) and then on a buckled graphene (Sec. IV B).

A. Rashba effect in ideal graphene

Without SO coupling, the band structure of graphene at a Dirac point consists of linear bands which show no band gap [Fig. 3(a)]. Including the SO interaction gives rise to an SO gap of 24.5 μeV [Fig. 3(b)], in agreement with the 24 μeV reported in Ref. 26. Our relativistic KKR calculations reproduce the above findings. They show further that the SO gap is reduced to less than 1 μeV if d and f orbitals are removed from the Fermi level, as predicted by Slonczewski and Weiss.[27] Or formulated differently, 96% of the SO-induced band gap are due to d and f contributions, although the latter contribute marginally to the density of states. These results confirm those of Ref. 26. Thus, by increasing the hybridization of the graphene π states with d or f states of a suitable substrate, one may increase the SO band gap substantially.

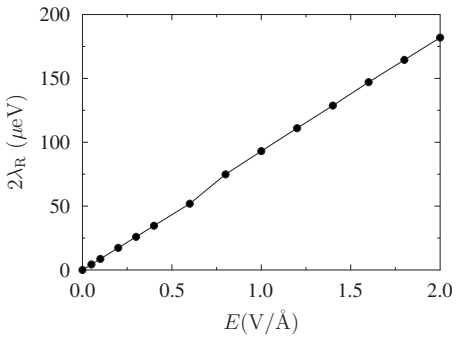

FIG. 4. Strength λ_R of the Rashba spin-orbit coupling in graphene versus strength of an external electric field (dots). The line serves as guide to the eyes.

Time-reversal and inversion symmetry imply that the bands are doubly degenerate, that is, $\epsilon(\uparrow,\vec{k})=\epsilon(\downarrow,\vec{k})$. An external electric field breaks the inversion symmetry and, consequently, the spin degeneracy is lifted. The resulting band topology deviates from those in conventional Rashba systems, e.g., surface states at metal surfaces,[28] but complies fully with the effective-mass model above. A reason is that at metal surface, the Rashba split states show up at the Brillouin zone center which is a time-reversal invariant point. In contrast, the Dirac points K (K') are not time-reversal invariant: K is turned into K' upon time reversal and vice versa.

The strength λ_R of the Rashba SO interaction is extracted from the band structure at K as $4\lambda_R=\varepsilon_{++}-\varepsilon_{--}$. For an external electric field of 0.1 V/Å, λ_R equals 4.34 μeV [Fig. 3(c)]. For all electric fields considered (Fig. 4), the band topologies (not shown here) are close to those of Ref. 26 in which also a FLAPW code was applied.

λ_R depends mostly linear on the applied electric field, in agreement with the effective-mass model and the calculations reported in Ref. 26. The SO band gap is within the order of hundreds of microelectron volt which is hardly to access in experiments and unlikely to be employed in device applications. Nevertheless, the relative change in the SO band, with respect to the zero-field case, indicates a significant electric field effect on graphene's electronic properties, despite its low carrier density.[2]

We now turn to the spin topology of Rashba-split bands, as obtained by the relativistic KKR method.[14] The Rashba SO interaction imposes that the spin polarization of the electronic states is complete (100%) in plane and normal to the wave vector.[26,29] This paradigmatic spin structure shows up in surface states at metal surfaces with minor deviations which are due to the surface symmetry.

This in-plane spin structure is found in graphene as well but at $\vec{k}$ off the Dirac points [Figs. 5(a) and 5(c)]. The spin can be viewed as rotating clockwise or anticlockwise around the Dirac cones, as is schematically sketched in Fig. 6. However, this spin structure cannot be maintained when approaching the Dirac point, which is readily seen by the vanishing spin polarization at $k=0$ in Figs. 5(a) and 5(c). As a consequence, the out-of-plane component P_z of the spin polarization which is small for large $|k|$ becomes $\pm 100\%$ at $k=0$ (K and K'). The resulting spin topology can be cast as

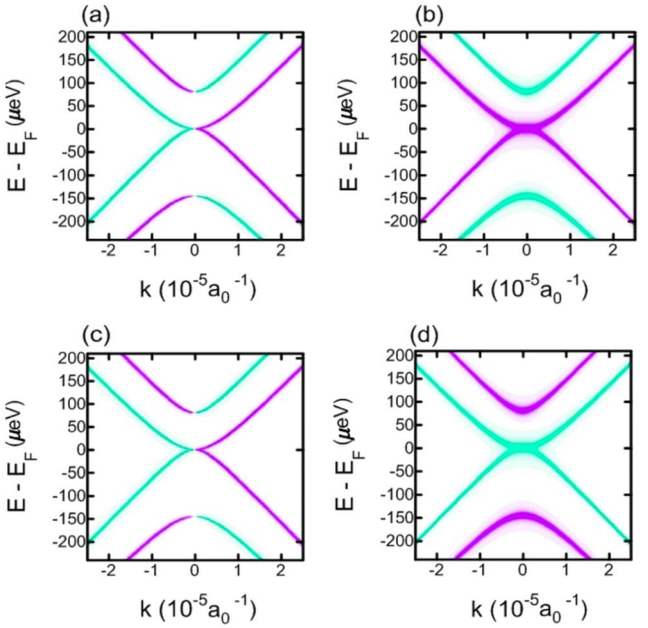

FIG. 5. (Color online) Spin-resolved band structure of graphene near K (K') with an external electric field of about 0.8 V/Å. The upper (a) left and (b) right panels represent the band structure near K for the spin quantization lying in-plane and out-of-plane (parallel to the surface normal), respectively. The lower panels, (c) and (d), are as (a) and (b) but near K'. The color (grayscale) distinguishes between the two spin projections while the thickness indicates the degree of the spin polarization.

spin vortices; two of them are schematically sketched in Fig. 6. This spin topology is due to the transition from the intrinsic (close to K) to the extrinsic (far away from K) SO dominated regions. Time-reversal symmetry implies $\vec{P}(k)=-\vec{P}(-k)$, leaving the system nonmagnetic. This is readily checked by comparing Figs. 5(a) and 5(c). It especially

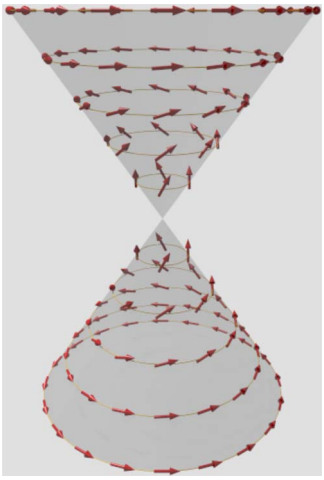

FIG. 6. (Color online) Perspective view of the spin topology of two Dirac cones at the K (schematic or artist's view). At large k offsets from K the spins (arrows) are in-plane [Fig. 5(a)] and rotate counterclockwise along the circular cuts of the Dirac cones. The spin are rotated increasingly out of the plane [Fig. 5(b)] when approaching the tip of a cone, leading to spin vortices.

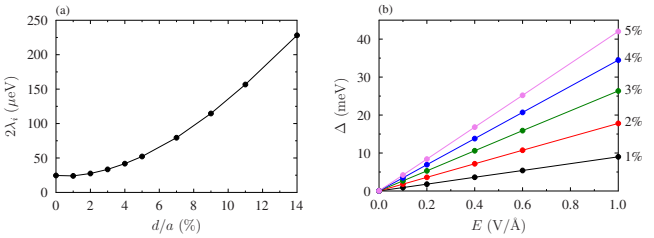

FIG. 7. (Color online) Spin-orbit coupling and fundamental SO band gap in mini-ripple graphene. (a) Intrinsic SO splitting λ_i versus buckling d. The latter is the z distance between A and B carbon atoms (sublattices), in units of the lattice constant a. (b) Fundamental SO band gap versus external electric field for $d/a = 1\%, \ldots, 5\%$ (as indicated). Lines are guides to the eyes.

yields $P_z(K) = -P_z(K')$ [Figs. 5(b) and 5(d)]. Our first-principles results match those of a tight-binding model.[30]

B. Rashba effect in buckled graphene

Graphene is usually manufactured on a substrate.[17,18] As consequence, its geometry can deviate from the honeycomb lattice by an in-plane deformation (i.e., strained graphene)—which is discussed in Sec. III—or by an outward relaxation of the C atoms. Since graphene is typically bonded weakly to a substrate, by the van der Waals interaction, the z displacements of the C sites is expected small and possibly not in registry with the substrate lattice. Further, ripples and corrugation are long ranged.[31,32] Thus, a realistic description of buckled graphene requires very large unit cells which is hardly manageable in first-principles calculations. Consequently, one has to rely on models for buckled graphene with small unit cells.

A simple model for buckled graphene is to break the equivalence of the A and B sublattices by shifting one carbon species out of lattice plane by a displacement d, leading to a "mini-ripple geometry." In ideal graphene, the σ (s, p_x, and p_y) and π orbitals (p_z) are not coupled, as is readily apparent from their zero overlap in a tight-binding picture. A displacement of an atom normal to the lattice plane makes the σ-π coupling nonzero, as was proven in Ref. 26, thus opening additional interaction "channels." Since the latter affect also the (intrinsic) SO-coupling strength λ_i,[33] we expect an increasing fundamental SO gap with buckling d. However, the increased band gap obtained within the "mini-ripple" model has to be regarded as an "upper limit" since this model has the most short-ranged corrugation.

The above reasoning is fully confirmed by the first-principles calculations [Fig. 7(a)]. The fundamental SO band gap of width $2\lambda_i$ [cf. Fig. 3(a)] increases parabolic with z-distance d of the A- and B-sublattice carbon atoms, confirming the results of Ref. 26. However, even at a sizable buckling of 14% the SO band gap is as small as 230 μeV.

Since an external electric field has a minor effect on the SO band gap (cf. Fig. 4), a question arises whether the latter can be increased by an interplay of buckling and electric field. We have therefore calculated the fundamental SO band gap for "mini-rippled" graphene for various external electric fields [Fig. 7(b)]. As already established for the zero-buckling case (Fig. 4), the SO gap increases linearly with field strength, even for buckled graphene. The striking result, however, is that the SO gap width is drastically increased upon buckling. For the zero-buckling case, the SO gap is about 100 μeV at 1 V/Å while for 5% buckled graphene it is larger than 40 meV; this is an enhancement by 2 orders of magnitude. Hence, we conclude that lattice distortions—either in plane or out of plane—increase the fundamental SO band gap, as compared to ideal graphene. The Rashba effect then allows to control the electronic properties at the Dirac point via an external electric field.

It is worth noticing here that for purely sp^3-hybridized carbon orbitals, e.g., diamond crystal, the SO splitting (the SO band gap) is about 6 meV,[34] and one could change the hybridization of graphene toward an sp^3, enhancing its SO splitting to the same order by displacing one of the carbon atoms from the plane.[35] This displacement can be induced by doping (see Sec. V). Indeed, according to Fig. 7 buckling enhances significantly the SO gap only when combined with electric field [Fig. 7(b)], meaning that the electric field-induced charge transfer is necessary to make an sp^3 hybridization with an SO splitting in the millielectron volt scale.

V. ELECTRON DOPING OF GRAPHENE BY ADATOMS

As has been noted in Sec. IV A, the SO-induced band gap is essentially due to d and f orbitals. Thus, by hybridization of graphene's π orbitals with d orbitals of adatoms or substrate atoms, one could increase the SO splitting, provided the band topology at the Dirac point is maintained. Another question is concerned with the position of the Fermi level which is affected by the hybridization as well. And eventually, one has to address the origin of a splitting which occurs upon adsorption of magnetic atoms (say, Ni): increased spin-orbit coupling or induced exchange splitting?

In this section we report on the electronic properties of graphene with adsorbed Au and Ni atoms. A quasi-free-standing graphene layer can be manufactured by Au intercalation, as in graphene/Au/Ni(111),[36] or by epitaxial growth on Ni(111).[37] Recently, it was shown that Au which is intercalated between graphene and a SiC substrate produces an efficiently decoupled graphene monolayer.[38]

In the following, we address the adsorption of half a monolayer of Au or Ni on graphene. The atoms are placed on top of one carbon species, leading to three atoms per unit cell (two carbon atoms, one adatom).[39] As a consequence, the equivalence of the carbon sublattices A and B is broken. The calculated equilibrium graphene-adatom distances are $6.41a_0$ for Au and $5.50a_0$ for Ni.

A. Au adatoms

The adsorption of Au on graphene does maintain the conelike band topology with linear dispersion (Fig. 8). It further induces an extrinsic contribution to the SO coupling (Rashba effect), as is apparent from the band topology at K. The latter agrees with that established for an external electric field (cf. Fig. 5). The strength λ_R of the extrinsic SO cou-

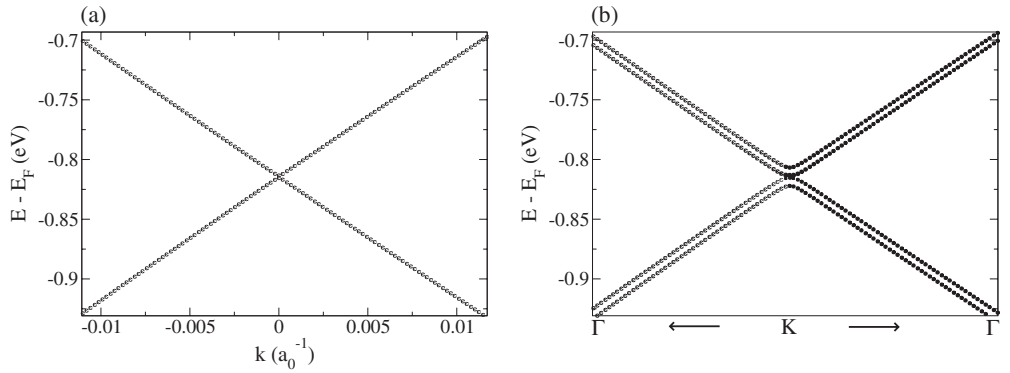

FIG. 8. Band structure of π states in graphene with $\frac{1}{2}$ of a monolayer of Au adsorbed (k relative to K), (a) without SO coupling and (b) including SO coupling.

pling is as large as 8 meV, which is about two orders of magnitude higher than for clean graphene with an external electric field of 1 V/Å. This result agrees with the measured Rashba-SO splitting of about 10 meV in graphene/Au/Ni(111) (Ref. 36) and with those calculated for different impurity coverages.[35] Furthermore, the similarity of the band structures representing the doping effect [Fig. 8(b)] and the electric field effect (Fig. 5) indicates that the charge-transfer mechanism is involved in both cases, i.e., charges transfer between the charged sheets and graphene when applying electric field and between the adatoms and carbon atoms when doping. Indeed, in the latter case, our results show that the charge-transfer process is dominated by the Au p-like charge transfer. This shows clearly that doping might be a useful technique to tune the Rashba-SO splitting into the millielectron volt scale at K.

The Dirac point is shifted down to E_F-808 meV, which agrees with the experimental shift of −850 meV that was found for graphene covered by $\frac{1}{3}$ of a monolayer of Au.[38] A shift to negative energies is a signature of n doping.

The shift ΔE_F of the Dirac point in graphene is shown in Fig. 9 (red small circles) as a function of the graphene-Au distance d. With decreasing distance, ΔE_F increases but remains negative (n doping) until $d=3.39a_0$ ($\frac{d-d_{Au}}{d_{Au}}=-47\%$). Here, p doping abruptly sets in, with $\Delta E_F=+564$ meV, suggesting that p doping occurs at distances $d\leq 3.46a_0$ (-46%). This supports the estimated experimental shift of the Dirac point by +100 meV claimed for p-doped graphene.[38]

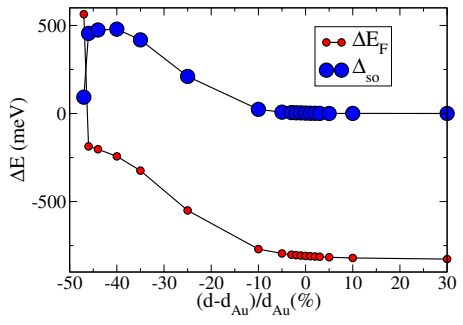

FIG. 9. (Color online) Electronic properties of graphene covered by $\frac{1}{2}$ of a monolayer of Au. The shift ΔE_F of the Dirac point with respect to the Fermi level E_F (red small circles) and the SO splitting Δ_{SO} at the Dirac point (blue big circles) are displayed versus Au-graphene distance (equilibrium distance $d_{Au}=6.41a_0$). Lines are guides to the eyes.

The spin-orbit splitting at the Dirac point (blue big circles in Fig. 9) follows the trend in ΔE_F. The above findings are in analogy to a semiconductor. For a semiconductor, the fundamental band gap increases with decreasing lattice parameter. As the semiconductor band gap opens up between bonding and antibonding states, the SO splitting (SO gap) in graphene is between the π and π^* states.

Eventually, we note that our results contrast recent VASP first-principles calculations[40] which show p doping when increasing d. With the information at hand, we can only speculate on the origin of this mismatch. In favor of our approach we like to add that the FLAPW results are reproduced by the independent KKR calculations.

B. Ni adatoms

The nearest-neighbor distance of $2.68a_0$ in graphene is close to that of Ni(111), $a_{Ni}/\sqrt{6}=2.71a_0$, leading to a lattice mismatch of 1.1%. Therefore, Ni(111) is used as a substrate for growing graphene of good quality.

The effect of Ni adatoms on graphene is twofold. First, they induce an extrinsic (Rashba) spin-orbit splitting in the π states of graphene, as was discussed for Au in the previous section. Nevertheless, Ni atoms are much lighter than those of Au atoms ($Z_{Ni}=28$ versus $Z_{Au}=79$), and they are thus not expected to induce a considerable Rashba spin-orbit splitting. Second, they induce an exchange splitting which was proven in a recent x-ray magnetic circular dichroism (XMCD) experiment.[41] It was found that the hybridization of the π states of graphene and the Ni $3d$ states induces a magnetic moment of about 0.05 $\mu_B-0.1$ μ_B per carbon atom. This issue has also been addressed recently by the photoemission experiments.[37,42]

Figure 10(a) displays the band structure of the π states of graphene with $\frac{1}{2}$ of a monolayer of Ni adsorbed without SO coupling. The band topology near the K (K') is very similar to that when applying an external field (Fig. 5). However, the induced spin splitting in the present case is attributed to exchange splitting (SO coupling switched off in the calculations), rather than to a Rashba SO coupling (Sec. IV A). The

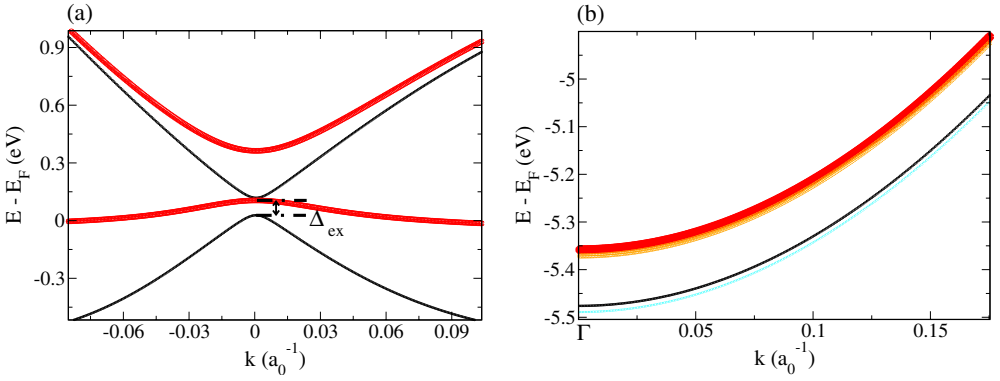

FIG. 10. (Color online) Electronic properties of graphene covered by $\frac{1}{2}$ of a monolayer of Ni. Band structure of π states close to the Fermi level (a) with k relative to K and (b) that of deep-laying π states at Γ. Colors differentiate between majority and minority spin bands, black thin and red thick bands represent the results without SO coupling, cyan thin and orange thick bands in panel (b) represent those including SO coupling.

dispersion of the graphene bands [Fig. 10(a)] follows that of the d bands of nickel (not shown here). Further, the deep-laying π states of graphene exhibit a similar behavior near Γ [Fig. 10(b)].

Including the SO coupling leads to a very similar band structure (not shown here) as compared to that without SO coupling [Fig. 10(a)]. The only visible effect of the SO interaction is a rigid shift of the bands of about 2 meV toward lower energies.

We conclude, therefore, that nickel has no effect on the SO coupling in graphene, neither on the bands at the Dirac point nor on the lower π bands. In particular the latter finding is in contrast to an experimental Rashba SO coupling of 225 meV for the π states at about 5.5 eV of bonding energy.[37] According to our calculations, a spin splitting is better ascribed to an induced exchange splitting,[42] rather than to a Rashba-type SO splitting. Further we note that a sizable Rashba-SO splitting is induced by heavy adatoms (here: Au).

In view of the linear dependence of the Rashba effect on the external electric field, one could imagine that heavy magnetic elements allow for a magnetoelectric control of graphene's electronic structure at the Dirac point. On one hand, it tunes the Rashba effect up to millielectron volt and is, on the other hand, susceptible to an external electric or magnetic field. In this respect, gadolinium[13] would be a promising candidate.

VI. CONCLUDING REMARKS

The first-principles calculations reported in this paper provide a comprehensive understanding of the bands in graphene at the Dirac point. The intrinsic (atomic) and the extrinsic (Rashba-type) spin-orbit coupling are too small to be employed in device applications *per se*. However, the results for deformed graphene—either in plane (here: toward a square lattice) or out-of-plane (here: in a mini-ripple model), lead to significantly increased band gaps or SO band gaps which then can be tuned by an external electric field. Likewise, the adsorption of heavy or magnetic element, such as Au and Ni, allows to increase the fundamental SO band gap and the SO spin splitting; thus, they provide a basis for further tuning the electronic structure by means of an external electric field. The present results call for experiments, in particular for spin-resolved photoelectron spectroscopy.

The joint effect of doping graphene by d electrons and of inducing a magnetic moment could open a path to modify the spin-dependent electronic structure of graphene, that is, by magnetoelectric coupling. Since Gd has d electrons close to the Fermi level and a large magnetic moment, it could be a promising candidate in designing new carbon-based spintronic devices.

ACKNOWLEDGMENTS

We appreciate fruitful discussions with G. Bihlmayer, H. Mirhosseini, and D. Böttcher. This work is supported by the Sonderforschungsbereich 762, "Functionality of Oxide Interfaces."

[1] A. Bostwick, T. Ohta, T. Seyller, K. Horn, and E. Rotenberg, Nat. Phys. **3**, 36 (2007).
[2] S. V. Morozov, K. S. Novoselov, F. Schedin, D. Jiang, A. A. Firsov, and A. K. Geim, Phys. Rev. B **72**, 201401(R) (2005).
[3] Y. Zhang, Y.-W. Tan, H. L. Stormer, and P. Kim, Nature (London) **438**, 201 (2005).
[4] M.-H. Liu, G. Bihlmayer, S. Blügel, and C.-R. Chang, Phys. Rev. B **76**, 121301(R) (2007).
[5] Y. A. Bychkov and E. I. Rashba, Sov Phys. JETP **39**, 78 (1984).
[6] Yu. M. Koroteev, G. Bihlmayer, J. E. Gayone, E. V. Chulkov, S. Blügel, P. M. Echenique, and Ph. Hofmann, Phys. Rev. Lett. **93**, 046403 (2004).
[7] C. R. Ast, J. Henk, A. Ernst, L. Moreschini, M. C. Falub, D. Pacilé, P. Bruno, K. Kern, and M. Grioni, Phys. Rev. Lett.

98, 186807 (2007).
[8] G. Bihlmayer, S. Blügel, and E. V. Chulkov, Phys. Rev. B **75**, 195414 (2007).
[9] H. Mirhosseini, I. V. Maznichenko, S. Abdelouahed, S. Ostanin, A. Ernst, I. Mertig, and J. Henk, Phys. Rev. B **81**, 073406 (2010).
[10] G. Liang, N. Neophytou, D. E. Nikonov, and M. S. Lundstrom, IEEE Trans. Electron Devices **54**, 677 (2007).
[11] http://www.flapw.de, see also S. Blügel and G. Bihlmayer, *Computational Nanoscience: Do It Yourself*, NIC Series Vol. 31 (John von Neumann Institute for Computing, Jülich, 2006), p. 85.
[12] V. L. Moruzzi, J. F. Janak, and A. R. Williams, *Calculated Electronic Properties of Metals* (Pergamon Press, New York, 1978).
[13] S. Abdelouahed, N. Baadji, and M. Alouani, Phys. Rev. B **75**, 094428 (2007).
[14] *Electron Scattering in Solid Matter*, in edited by J. Zabloudil, R. Hammerling, L. Szunyogh, and P. Weinberger (Springer, Berlin, 2005).
[15] J. Henk, in *Handbook of Thin Film Materials*, edited by H. S. Nalwa (Academic Press, San Diego, 2001), Vol. 2, Chap. 10, p. 479.
[16] J. P. Perdew and Y. Wang, Phys. Rev. B **45**, 13244 (1992).
[17] K. S. Novoselov, A. K. Geim, S. V. Morozov, D. Jiang, M. I. Katsnelson, I. V. Grigorieva, S. V. Dubonos, and A. A. Firsov, Nature **438**, 197 (2005).
[18] C. Berger, Z. Song, X. Li, X. Wu, N. Brown, C. Naud, D. Mayou, T. Li, J. Hass, A. N. Marchenkov, E. H. Conrad, P. N. First, and W. A. de Heer, Science **312**, 1191 (2006).
[19] R. M. Ribeiro, V. M. Pereira, N. M. R. Peres, P. R. Briddon, and A. H. Castro Neto, New J. Phys. **11**, 115002 (2009).
[20] J. Buschbeck, I. Opahle, M. Richter, U. K. Rößler, P. Klaer, M. Kallmayer, H. J. Elmers, G. Jakob, L. Schultz, and S. Fähler, Phys. Rev. Lett. **103**, 216101 (2009).
[21] S. Y. Zhou, G.-H. Gweon, A. V. Fedorov, P. N. First, W. A. de Heer, D.-H. Lee, F. Guinea, A. H. Castro Neto, and A. Lanzara, Nature Mater. **6**, 770 (2007).
[22] S. Datta and B. Das, Appl. Phys. Lett. **56**, 665 (1990).
[23] F. Reinert, J. Phys.: Condens. Matter **15**, S693 (2003).
[24] D. P. DiVincenzo and E. J. Mele, Phys. Rev. B **29**, 1685 (1984).
[25] C. L. Kane and E. J. Mele, Phys. Rev. Lett. **95**, 226801 (2005).
[26] M. Gmitra, S. Konschuh, C. Ertler, C. Ambrosch-Draxl, and J. Fabian, Phys. Rev. B **80**, 235431 (2009).
[27] J. C. Slonczewski and P. R. Weiss, Phys. Rev. **109**, 272 (1958).
[28] J. Henk, A. Ernst, and P. Bruno, Phys. Rev. B **68**, 165416 (2003).
[29] E. I. Rashba, Phys. Rev. B **79**, 161409(R) (2009).
[30] M.-H. Liu and C.-R. Chang, Phys. Rev. B **80**, 241304(R) (2009).
[31] A. Fasolino, J. H. Los, and M. I. Kastnelson, Nature Mater. **6**, 858 (2007).
[32] F. Guinea, M. I. Katsnelson, and M. A. H. Vozmediano, Phys. Rev. B **77**, 075422 (2008).
[33] C. Ammer, K. Meinel, H. Wolter, A. Beckmann, and H. Neddermeyer, Surf. Sci. **375**, 302 (1997).
[34] P. Y. Yu and M. Cardona, *Fundamentals of Semiconductors: Physics and Materials Properties* (Springer, New York, 2005).
[35] A. H. Castro Neto and F. Guinea, Phys. Rev. Lett. **103**, 026804 (2009).
[36] A. Varykhalov, J. Sanchez-Barriga, A. M. Shikin, C. Biswas, E. Vescovo, A. Rybkin, D. Marchenko, and O. Rader, Phys. Rev. Lett. **101**, 157601 (2008).
[37] Y. S. Dedkov, M. Fonin, U. Rüdiger, and C. Laubschat, Phys. Rev. Lett. **100**, 107602 (2008).
[38] I. Gierz, T. Suzuki, R. T. Weitz, D. S. Lee, B. Krauss, C. Riedl, U. Starke, H. Höchst, J. H. Smet, C. R. Ast, and K. Kern, Phys. Rev. B **81**, 235408 (2010).
[39] G. Bertoni, L. Calmels, A. Altibelli, and V. Serin, Phys. Rev. B **71**, 075402 (2005).
[40] G. Giovannetti, P. A. Khomyakov, G. Brocks, V. M. Karpan, J. van den Brink, and P. J. Kelly, Phys. Rev. Lett. **101**, 026803 (2008).
[41] M. Weser, Y. Rehder, K. Horn, M. Sicot, M. Fonin, A. B. Preobrajenski, E. N. Voloshina, E. Georing, and Y. S. Dedkov, Appl. Phys. Lett. **96**, 012504 (2010).
[42] O. Rader, A. Varykhalov, J. Sanchez-Barriga, D. Marchenko, A. Rybkin, and A. M. Shikin, Phys. Rev. Lett. **102**, 057602 (2009).